The Effect of the Thermosphere on Ionosphere Outflows

J. Krall[1]* and J. D. Huba[2]

[1]*Naval Research Laboratory, Plasma Physics Division, Washington, DC, United States,* [2]*Syntek Technologies, Fairfax, VA, United States*

The Naval Research Laboratory (NRL) Sami2 is Another Model of the Ionosphere (SAMI2) and Sami3 is Also a Model of the Ionosphere (SAMI3) ionosphere/plasmasphere codes have shown that thermosphere composition and winds significantly affect H$^+$ outflows from the topside ionosphere. In particular, O density inhibits upward diffusion of O$^+$ from the ionosphere F layer, especially during solar maximum conditions. In addition, winds affect the quiet-time latitudinal extent of the F layer, affecting densities at mid-to-high latitudes that are the source of plasmasphere refilling outflows. Evidence for these effects is reviewed and prospects for forecasting these outflows are explored. Open questions for future research are highlighted.

Keywords: ionosphere, plasmasphere, thermosphere, ionosphere outflow, cold plasma, exosphere

1 INTRODUCTION

Light ions, H$^+$ and He$^+$, commonly flow upward from the topside ionosphere. At high latitudes, these ions constitute the classical polar wind (Bauer and Frihagen, 1966; Dessler and Michel, 1966). At lower latitudes, these outflows fill the plasmasphere (Park, 1970; Gallagher and Comfort, 2016). Because the polar wind and plasmasphere serve as a source and a sink, respectively, for geoeffective energetic ions, thermal (non-energized, Maxwellian) outflows are essential elements of space weather (Bortnik and Thorne, 2007; Millan and Thorne, 2007). Further, observations suggest significant day-to-day variability in thermosphere composition (Krall et al., 2016a; Cai et al., 2020) and winds (McDonald et al., 2015). In this brief review, we consider the effect of thermosphere composition and winds on refilling outflows. Thermosphere dynamics and ionosphere outflows at polar latitudes, a much bigger subject, will not be addressed.

Because the solar cycle so strongly affects thermosphere and exosphere composition, the variation of cold H$^+$ refilling outflows with the solar cycle, specifically with the $F_{10.7}$ extreme ultraviolet (EUV) index, is quite counter-intuitive. At high $F_{10.7}$, when the ionosphere F layer is relatively strong, observed plasmasphere refilling rates at geosynchronous altitudes are relatively weak (Lawrence et al., 1999; Gallagher et al., 2021). As shown graphically in **Figure 1D**, and described by Richards and Torr (1985), the limiting H$^+$ outflow flux is proportional to the supply of O$^+$ ions and H atoms at outflow source height Z_0 (700–1,100 km):

$$\phi\,[\mathrm{cm^{-2}s^{-1}}] = 2.85 \times 10^{-11}\, T_n\,[\mathrm{K}]^{1/2}\, n_H\,[\mathrm{cm^{-3}}]\, n_{O^+}\,[\mathrm{cm^{-3}}]\, H_{O^+}\,[\mathrm{cm}], \tag{1}$$

where T_n is the thermosphere temperature, H_{O^+} is the O$^+$ scale height, and the leading coefficient has been updated from 2.50 to 2.85 based on a corresponding update to the H-O$^+$ charge exchange reaction rate. Previously, the H-O$^+$ charge exchange reaction rate was based on data for the reverse
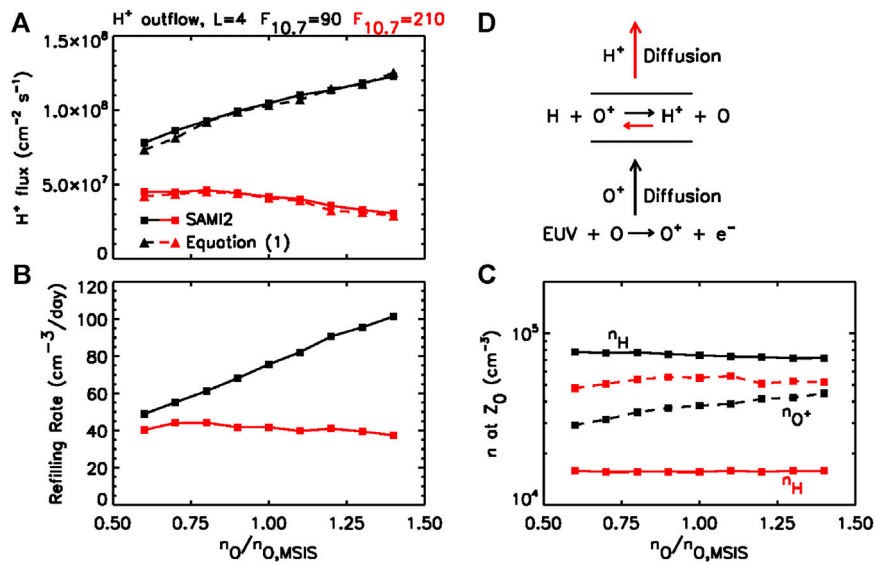
FIGURE 1 | (A) H^+ flux from SAMI2 and from **Eq. 1 (B)** refilling rate, and **(C)** n_H and n_{O^+}, plotted vs. $n_O/n_{O,MSIS}$. Black curves are for low solar activity, $F_{10.7} = 90$. Red curves are for high solar activity, $F_{10.7} = 210$. **(D)** Diagram showing the production and upward diffusion of O^+ and H^+ ions. The O density inhibits upward diffusion; this sensitivity to the O density is not explicit in **Eq. 1**. Note: these results (Krall and Huba, 2019a) use 2.50 instead of 2.85 in **Eq. 1** and in the charge-exchange rate.

reaction (Fehsenfeld and Ferguson, 1972) and the finding that the ratio of the forward to reverse reaction rates is 9/8 (Hanson and Ortenburger, 1961). However, recent analysis (Stancil et al., 1999) and measurements (Waldrop et al., 2006; Joshi and Waldrop, 2019) suggest that this ratio is somewhat ($\simeq 14\%$) larger, increasing the coefficient in the reaction rate, and in **Eq. 1**, from 2.50 to 2.85.

Let us consider the factors in **Eq. 1**. Relative to densities at solar minimum (low $F_{10.7}$), n_H at solar maximum is much lower (Bishop et al., 2001; Bishop et al., 2004; Nossal et al., 2012; Qian et al., 2018) while n_{O^+} is only somewhat higher (this is at altitude Z_0, which increases with $F_{10.7}$). These densities are shown in **Figure 1C**, where high $F_{10.7}$ is indicated by red curves. This basic understanding of thermal ion outflows, particularly as expressed in **Eq. 1**, compares well to simulations (Richards and Torr, 1985; Krall and Huba, 2019a). However, we are not yet able to forecast these outflows.

In addition, the ionosphere F layer that is the source of these outflows is strongly affected by thermosphere winds (Rishbeth, 1998). Specifically, winds effect the degree to which the ionosphere, which is most strongly generated near the sub-solar point, is transported to the mid-to-high latitudes that are the source of the plasmasphere. While numerical simulations by Krall et al. (2014) demonstrate that plasmasphere morphology and refilling rates are impacted by thermosphere winds, these effects have yet to be directly observed. As it stands, measured post-storm plasmasphere refilling rates at any given height vary by as much as an order of magnitude (Denton et al., 2012), **Figure 1**. These variations are not yet fully explained.

This brief review is based on results from the Sami2 is Another Model of the Ionosphere (SAMI2) and Sami3 is Also a Model of the Ionosphere (SAMI3) ionosphere/plasmasphere codes (Huba et al., 2000; Huba and Krall, 2013). SAMI3 simulates the interaction between ionosphere and plasmasphere ion populations and the thermosphere (Huba and Liu, 2020) and magnetosphere (Huba et al., 2005; Huba and Sazykin, 2014). SAMI2 solves the same equations as SAMI3, but in only a single magnetic longitude. For the results included here, SAMI2 was modified to accommodate counterstreaming H^+ outflows as in Krall and Huba (2019b).

In the next section, the effect of thermosphere composition, particularly the O density, will be demonstrated using SAMI2. This will be followed by SAMI3 results showing the effect of winds. We then discuss the challenge of forecasting these outflows, given observed day-to-day variability in thermosphere composition and winds. We close with a brief list of open questions for future research.

2 SAMI2 RESULTS: THERMOSPHERE COMPOSITION

In a recent simulation (Krall et al., 2016b) of post-storm plasmasphere refilling (Singh and Horwitz, 1992), it was found that model-data agreement was not attainable without careful attention to the thermosphere O density. In particular, O atoms tend to act as a barrier to the upward diffusion of O^+ ions (**Figure 1D**). This effect, which is not explicit in **Eq. 1**, was recently illustrated using the SAMI2 code (Krall and Huba,
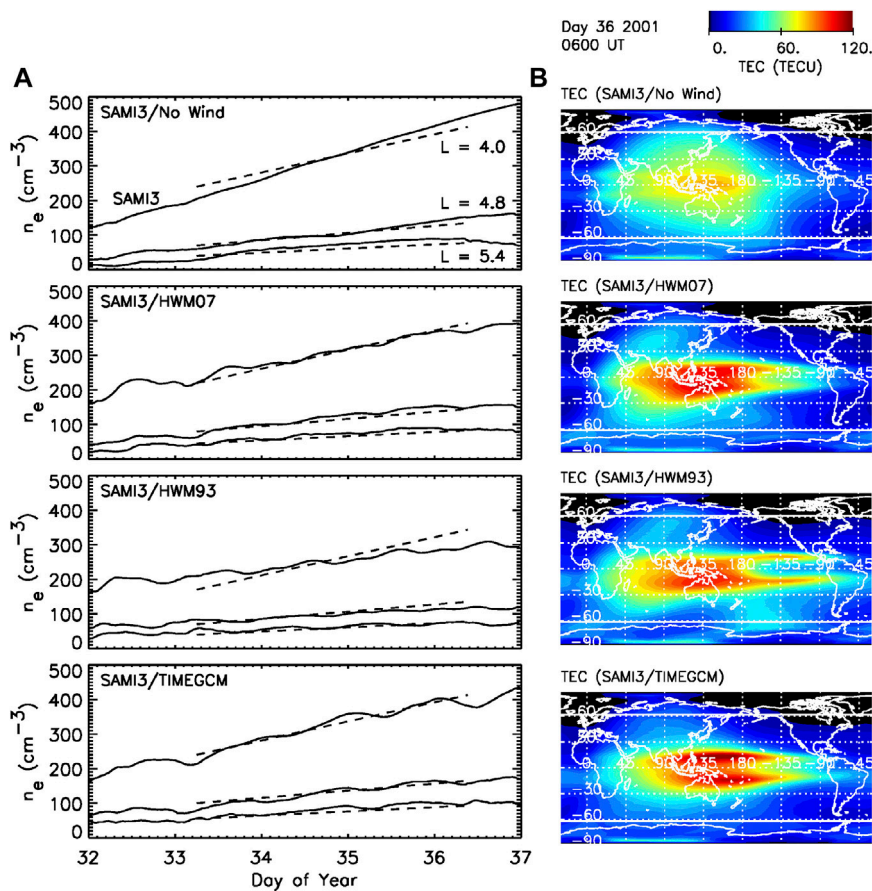
FIGURE 2 | Left column: electron density averaged over longitude in the equatorial plane plotted vs. time for L = 4.0, 4.8 and 5.4 (solid curves) for SAMI3/No Wind, SAMI3/HWM07, SAMI3/HWM93 and SAMI3/TIMEGCM. Dashed lines in each plot indicate observed refilling rates. Right column: total electron content in TEC units is plotted vs. longitude and latitude at 0600 UT on Day 36 for each case. White lines indicate latitude $\pm 61.5°$ (L = 4.8).

2019a). The SAMI2 code, which simulates a single magnetic-longitude plane, runs quickly enough to support parameter studies such as described here.

In a series of simulations of outflow and refilling following a model storm, the thermosphere O density was varied relative to values provided by the NRLMSISE-00 (Picone et al., 2002) version of the Magnetic Spectrometer Incoherent Scatter (MSIS) empirical atmosphere model (Hedin, 1987). This was done for solar maximum ($F_{10.7}$ = 210) and minimum ($F_{10.7}$ = 90) conditions. In this study we recorded conditions at outflow source height Z_0, values computed using **Eq. 1**, and the simulated outflow flux above Z_0. At height Z_0, an H^+ ion has an equal chance of being lost to charge exchange or to outflow; these processes are indicated by red arrows in **Figure 1D**.

The results are presented in **Figure 1**. In **Figure 1C**, n_H and n_{O^+} at the outflow source height are plotted vs. $n_O/n_{O,MSIS}$. Note that the much lower value of n_H at $F_{10.7}$ = 210 accounts for the counter-intuitive result that outflow fluxes are smaller at solar maximum, when the ionosphere is strongest.

Increased O levels in the thermosphere affect outflows in two ways, both of which are illustrated in **Figures 1A,B**. First, increased O increases the O supply in the ionosphere. At solar

minimum (black curves), this effect dominates; note the increase in O^+ in **Figure 1C**. Second, increased O slows the upward diffusion of O^+. At solar maximum (red curves) the diffusion effect tends to dominate, slowing outflow and refilling. Further results (Krall and Huba, 2019a)], show that the O^+ scale height falls with increasing n_O, but only for solar maximum conditions.

Good agreement between SAMI2 and **Eq. 1**, shown in **Figure 1A**, demonstrates that the effect of the O density is fully consistent with the outflow formulation of Richards and Torr (1985).

3 SAMI3 RESULTS: THERMOSPHERE WINDS

We now consider the effect of thermosphere winds on plasmasphere refilling. As is well known (Rishbeth, 1998; Lühr et al., 2011), the wind-driven dynamo potential drives E × B drifts that affect the buildup of plasma density in the ionosphere. The impact of wind-driven ionosphere variability on plasmasphere refilling was demonstrated in Krall et al. (2014). Here, SAMI3

simulations were shown to compare well to *in situ* measurements of plasmasphere n_e during post-storm refilling, with model-data agreement improving as the thermosphere component of the simulation was improved.

In order to run SAMI3 (or SAMI2), thermosphere densities and winds must be specified. Typically, as in the SAMI2 runs above, we compute densities using MSIS (Hedin, 1987; Picone et al., 2002) and compute winds using the Horizontal Wind Model (Hedin, 1991; Drob et al., 2008; Drob et al., 2015). However, we can instead obtain a thermosphere specification from a first-principles model, such as the Thermosphere Ionosphere Mesosphere Electrodynamics General Circulation Model (TIMEGCM) (Roble and Ridley, 1994). For the results presented here TIMEGCM was driven, at the lower boundary, by climatological tides.

In each of the SAMI3 simulations of Krall et al. (2014), and **Figure 2**, we model five days of refilling following a geomagnetic storm on day 31 of 2001. **Figure 2** (left column) shows refilling as globally averaged n_e at the apex of $L = 4.0$, 4.8, and 5.0 field lines, where L is the McIlwain parameter (McIlwain, 1961). Globally averaged n_e (solid curves) are compared to global refilling rates based on *in situ* measurements (dashed lines) for a variety of thermosphere models: MSIS/No Wind, MSIS/HWM07, MSIS/HWM93 and TIMEGCM. The most realistic model, TIMEGCM, gives the best results; MSIS/HWM07 also works well.

The state of the ionosphere for each case is shown in the right-hand column, where Total Electron Content (vertically integrated n_e) is plotted vs. latitude and longitude at a fixed time. Of interest is the strength of the ionosphere at the mid-to-high latitude source of refilling. In each plot, a horizontal line at latitude $\pm 61.5°$ indicates the source of refilling for $L = 4.8$ (in this version of SAMI3, the geomagnetic field is modeled as an aligned dipole; geographic and geomagnetic coordinates are the same). We see that the case with the strongest refilling (No Wind) has the strongest ionosphere TEC values at this relatively high latitude.

4 DISCUSSION: CAN THESE EFFECTS BE FORECASTED?

Any event that affects thermosphere O densities, exosphere H densities, or thermosphere winds on a global scale, such as a geomagnetic storm or a sudden stratosphere warming (SSW) (Chau et al., 2009; Oberheide et al., 2020), has the potential to affect global refilling rates. For example, Jones et al. (2020) suggests that both SSW events and magnetospheric cooling events affect the density of H atoms in the exobase. In order to understand and predict outflows, it is necessary to understand and predict these episodic events.

In addition, thermosphere observations (McDonald et al., 2015; Cai et al., 2020) suggest significant day-to-day variability. For example, satellite data can be used to estimate the globally averaged O density at altitude 400 km, where O is the dominant atom (Picone et al., 2005). In Krall et al. (2016a), Figure 3, we presented such data with a 4-day resolution, finding that global n_O varies by $\pm 16\%$ on time scales of less than 30 days.

Lei et al. (2008) analyzed similar data, finding density oscillations with periods of 7 and 9 days. While these data do not demonstrate day-to-day variability, they are suggestive. Further, because tides transport O density (Jones et al., 2014), wind variability could be a source of density variability.

Day-to-day variability of thermosphere winds can be observed in daily measurements of TEC. McDonald et al. (2015) presented such TEC data and showed that, when driven from below by assimilated data, a computer simulation of the thermosphere reproduces about 50% of the observed variability. This forcing from below (McCormack et al., 2017) and resulting impacts (Jones et al., 2014) are increasingly well-understood in terms of tides. Specific mechanisms, such as tidal amplification (Goncharenko et al., 2010; Klimenko et al., 2019) and specific ionosphere signatures (Immel et al., 2006) have been identified. While older simulations (Fang et al., 2013) support the finding that tidal forcing accounts for about one half of observed variability, recent work (Zawdie et al., 2020) comes closer to determining the state of the ionosphere-thermosphere system in enough detail to now-cast the upper-atmospheric source of refilling outflows.

While even less is known about day-to-day variability in the exosphere, recent results are suggestive. For example, climatological analysis of exosphere observations revealed both solar cycle dependence and significant scatter, perhaps indicative of variability (Joshi et al., 2019). Diurnal variability has been quantified (Qian et al., 2018), but does not necessarily imply day-to-day variability. Perhaps more to the point, Forbes et al. (2014) found that signatures of thermosphere tides are detectable in exosphere temperatures. This implies that day-to-day variability in thermosphere tides, which is known to be present for some tidal components, might be a cause of similar variability in exosphere H densities. If present, day-to-day variability in exosphere H densities could contribute to the observed scatter in refilling rates (Krall et al., 2018). Finally, we note that the exosphere could have structure (Hodges, 1994; Cucho-Padin and Waldrop, 2018) not present in these simulations, especially during a storm (Kuwabara et al., 2017; Qin et al., 2017; Zoennchen et al., 2017; Cucho-Padin and Waldrop, 2019).

Simulations suggest that variability in thermosphere winds also affects global $E \times B$ drifts in the inner magnetosphere so as to affect the shape of the plasmasphere. Specifically, the Krall et al. (2014) study of **Figure 2**, showed that, when one wind model was exchanged for another, the shape of the model plasmasphere changed. Recent simulations showing model-data agreement for ionosphere/thermosphere interactions on a global scale (Huba and Liu, 2020) suggest that such modeling might soon reproduce ducts, crenelations, and other elements of observed plasmasphere structure (Horwitz et al., 1990). Numerical modeling that self-consistently couples the ionosphere and exosphere (Joshi and Waldrop, 2019) could also bring significant progress. Note that, at the cost of a small time step (about 1 s), SAMI3 does not suffer from the limitations of the diffusive equilibrium approximation (Huba and Joyce, 2014; Ozhogin et al., 2014), and has obtained reasonable model-data agreement (Krall et al., 2014; Krall et al., 2016b) for refilling events. Kinetic treatments (Wang et al., 2015) might prove valuable in validating these results. In addition, a current global

kinetic model, such as Pierrard and Stegen (2008), if coupled to a thermosphere model, might validate the finding (Krall et al., 2014) that the wind-driven dynamo affects the shape of the plasmasphere.

Finally, we should acknowledge that any forecast depends on accurate model inputs. Both satellite (Emmert, 2015) and Arecibo radar data (Joshi et al., 2018) show significant long-term deviations from the MSIS model. New observations of thermosphere winds on a global scale are presently coming from the NASA Ionospheric Connection Explorer (ICON) (Immel et al., 2018). ICON is equipped with a Michelson interferometer, built by the NRL, that measures winds and temperatures in the altitude range 90–300 km (Harding et al., 2021; Makela et al., 2021). We are hopeful that newly accurate thermosphere now-casting data products might be developed.

We close with a list of interesting open questions. What is the magnitude of day-to-day variability, if any, in the thermosphere O density? Does day-to-day variability of thermosphere densities, if any, imply similar variability in the exosphere? Do thermosphere winds truly shape the plasmasphere? How do high-latitude storm-driven winds affect the global wind-driven dynamo and refilling outflows?

AUTHOR CONTRIBUTIONS

Both JK and JH contributed to this work.

FUNDING

ACKNOWLEDGMENTS

REFERENCES

Bauer, S. J. (1966). "The Structure of the Topside Ionosphere," in *Electron Density Profiles in Ionosphere and Exosphere*. Editor J. Frihagen (New York: North-Holland), 387.

Bishop, J., Harlander, J., Nossal, S., and Roesler, F. L. (2001). Analysis of Balmer α Intensity Measurements Near Solar Minimum. *J. Atmos. Solar-Terrestrial Phys.* 63, 341–353. doi:10.1016/S1364-6826(00)00212-1

Bishop, J., Mierkiewicz, E. J., Roesler, F. L., Gómez, J. F., and Morales, C. (2004). Data-model Comparison Search Analysis of Coincident PBO Balmer α, EURD Lyman β Geocoronal Measurements from March 2000. *J. Geophys. Res.* 109, 1–9. doi:10.1029/2003JA010165

Bortnik, J., and Thorne, R. M. (2007). The Dual Role of ELF/VLF Chorus Waves in the Acceleration and Precipitation of Radiation belt Electrons. *J. Atmos. Solar-Terrestrial Phys.* 69, 378–386. doi:10.1016/j.jastp.2006.05.030

Cai, X., Burns, A. G., Wang, W., Qian, L., Solomon, S. C., Eastes, R. W., et al. (2020). The Two-Dimensional Evolution of Thermospheric σO/N Response to Weak Geomagnetic Activity during Solar-Minimum Observed by GOLD. *Geophys. Res. Lett.* 47, e2020GL088838. doi:10.1029/2020GL088838

Chau, J. L., Fejer, B. G., and Goncharenko, L. P. (2009). Quiet Variability of Equatorial E x B Drifts during a Sudden Stratospheric Warming Event. *Geophys. Res. Lett.* 36, 1–4. doi:10.1029/2008GL036785

Cucho-Padin, G., and Waldrop, L. (2019). Time-dependent Response of the Terrestrial Exosphere to a Geomagnetic Storm. *Geophys. Res. Lett.* 46, 11661–11670. doi:10.1029/2019GL084327

Cucho-Padin, G., and Waldrop, L. (2018). Tomographic Estimation of Exospheric Hydrogen Density Distributions. *J. Geophys. Res. Space Phys.* 123, 5119–5139. doi:10.1029/2018JA025323

Denton, R. E., Wang, Y., Webb, P. A., Tengdin, P. M., Goldstein, J., Redfern, J. A., et al. (2012). Magnetospheric Electron Density Long Term (Day) Refilling Rates Inferred from Passive Radio Emissions Measured by IMAGE RPI during Geomagnetically Quiet Times. *J. Geophys. Res.* 117, A03221. doi:10.1029/2011JA017274

Dessler, A. J., and Michel, F. C. (1966). Plasma in the Geomagnetic Tail. *J. Geophys. Res.* 71, 1421–1426. doi:10.1029/JZ071i005p01421

Drob, D. P., Emmert, J. T., Meriwether, J. W., Makela, J. J., Doornbos, E., Conde, M., et al. (2015). An Update to the Horizontal Wind Model (HWM): The Quiet Time Thermosphere. *Earth Space Sci.* 2, 301–319. doi:10.1002/2014EA000089

Drob, D. P., Emmert, T. J., Crowley, G., Picone, M. J., Shepherd, G. G., Skinner, W., et al. (2008). An Empirical Model of the Earth's Horizontal Wind fields: HWM07. *J. Geophys. Res. Space Phys.* 113, A12304. doi:10.1029/2008JA013668

Emmert, J. T. (2015). Altitude and Solar Activity Dependence of 1967–2005 Thermospheric Density Trends Derived from Orbital Drag. *J. Geophys. Res. Space Phys.* 120, 2940–2950. doi:10.1002/2015JA021047

Fang, T.-W., Akmaev, R., Fuller-Rowell, T., Wu, F., Maruyama, N., and Millward, G. (2013). Longitudinal and Day-To-Day Variability in the Ionosphere from Lower Atmosphere Tidal Forcing. *Geophys. Res. Lett.* 40, 2523–2528. doi:10.1002/grl.50550

Fehsenfeld, F. C., and Ferguson, E. E. (1972). Thermal Energy Reaction Rate Constants for H and CO with O and NO. *J. Chem. Phys.* 56, 3066–3070. doi:10.1063/1.1677642

Forbes, J., Zhang, X., and Bruinsma, S. (2014). New Perspectives on Thermosphere Tides: 2. Penetration to the Upper Thermosphere. *Earth, Planets and Space* 66, 122. doi:10.1186/1880-5981-66-122

Gallagher, D. L., Comfort, R. H., Katus, R. M., Sandel, B. R., Fung, S. F., and Adrian, M. L. (2021). The Breathing Plasmasphere: Erosion and Refilling. *J. Geophys. Res. Space Phys.* 126, e2020JA028727. doi:10.1029/2020JA028727

Gallagher, D. L., and Comfort, R. H. (2016). Unsolved Problems in Plasmasphere Refilling. *J. Geophys. Res. Space Phys.* 121, 1447–1451. doi:10.1002/2015JA022279

Goncharenko, L. P., Chau, J. L., Liu, H.-L., and Coster, A. J. (2010). Unexpected Connections between the Stratosphere and Ionosphere. *Geophys. Res. Lett.* 37, 1-6. doi:10.1029/2010GL043125

Hanson, W. B., and Ortenburger, I. B. (1961). The Coupling between the Protonosphere and the normal F Region. *J. Geophys. Res.* 66, 1425–1435. doi:10.1029/JZ066i005p01425

Harding, B. J., Chau, J. L., He, M., Englert, C. R., Harlander, J. M., Marr, K. D., et al. (2021). Validation of ICON-MIGHTI Thermospheric Wind Observations: 2. Green-line Comparisons to Specular Meteor Radars. *J. Geophys. Res. Space Phys.* 126, e2020JA028947. doi:10.1029/2020JA028947

Hedin, A. E. (1987). MSIS-86 Thermospheric Model. *J. Geophys. Res. Space Phys.* 92, 4649–4662. doi:10.1029/JA092iA05p04649

Hedin, A. E. (1991). Revised Global Model of Thermosphere Winds Using Satellite and Ground-Based Observations. *J. Geophys. Res. Space Phys.* 96, 7657–7688. doi:10.1029/91JA00251

Hodges, R. R. (1994). Monte Carlo Simulation of the Terrestrial Hydrogen Exosphere. *J. Geophys. Res. Space Phys.* 99, 23229–23247. doi:10.1029/94JA02183

Horwitz, J. L., Comfort, R. H., and Chappell, C. R. (1990). A Statistical Characterization of Plasmasphere Density Structure and Boundary Locations. *J. Geophys. Res. Space Phys.* 95, 7937–7947. doi:10.1029/JA095iA06p07937

Huba, J. D., Joyce, G., and Fedder, J. A. (2000). Sami2 Is Another Model of the Ionosphere (Sami2): A New Low-Latitude Ionosphere Model. *J. Geophys. Res.* 105, 23035–23053. doi:10.1029/2000JA000035

Huba, J. D., and Joyce, G. (2014). *Numerical Methods in Modeling the Ionosphere.* Washington, DC: American Geophysical Union, 49–55. chap. 5. doi:10.1002/9781118704417.ch5

Huba, J. D., Joyce, G., Sazykin, S., Wolf, R., and Spiro, R. (2005). Simulation Study of Penetration Electric Field Effects on the Low- to Mid-latitude Ionosphere. *Geophys. Res. Lett.* 32, 1–4. doi:10.1029/2005GL024162

Huba, J. D., and Krall, J. (2013). Modeling the Plasmasphere with Sami3. *Geophys. Res. Lett.* 40, 6–10. doi:10.1029/2012GL054300

Huba, J. D., and Liu, H.-L. (2020). Global Modeling of Equatorial Spread F with Sami3/WACCM-X. *Geophys. Res. Lett.* 47, e2020GL088258. doi:10.1029/2020GL088258

Huba, J. D., and Sazykin, S. (2014). Storm Time Ionosphere and Plasmasphere Structuring: Sami3-RCM Simulation of the 31 March 2001 Geomagnetic Storm. *Geophys. Res. Lett.* 41, 8208–8214. doi:10.1002/2014GL062110

Immel, T. J., England, S. L., Mende, S. B., Heelis, R. A., Englert, C. R., Edelstein, J., et al. (2018). The Ionospheric Connection Explorer Mission: Mission Goals and Design. *Space Sci. Rev.* 214, 1–4. doi:10.1007/s11214-017-0449-2

Immel, T. J., Sagawa, E., England, S. L., Henderson, S. B., Hagan, M. E., Mende, S. B., et al. (2006). Control of Equatorial Ionospheric Morphology by Atmospheric Tides. *Geophys. Res. Lett.* 33. doi:10.1029/2006GL026161

Jones, M., Jr., Forbes, J. M., Hagan, M. E., and Maute, A. (2014). Impacts of Vertically Propagating Tides on the Mean State of the Ionosphere-Thermosphere System. *J. Geophys. Res. Space Phys.* 119, 2197–2213. doi:10.1002/2013JA019744

Jones, M., Jr., Siskind, D. E., Drob, D. P., McCormack, J. P., Emmert, J. T., Dhadly, M. S., et al. (2020). Coupling from the Middle Atmosphere to the Exobase: Dynamical Disturbance Effects on Light Chemical Species. *J. Geophys. Res. Space Phys.* 125, e2020JA028331. doi:10.1029/2020JA028331

Joshi, P. P., Phal, Y. D., and Waldrop, L. S. (2019). Quantification of the Vertical Transport and Escape of Atomic Hydrogen in the Terrestrial Upper Atmosphere. *J. Geophys. Res. Space Phys.* 124, 10468–10481. doi:10.1029/2019JA027057

Joshi, P. P., Waldrop, L. S., and Brum, C. G. M. (2018). Ionospheric O Momentum Balance through Charge Exchange with Thermospheric O Atoms. *J. Geophys. Res. Space Phys.* 123, 9743–9761. doi:10.1029/2018JA025821

Joshi, P., and Waldrop, L. (2019). Parametric Estimation of Neutral Hydrogen Density under Charge Exchange and Quantification of its Effect on Plasmasphere-Ionosphere Coupling. *Earth Space Sci. Open Archive.* doi:10.1002/essoar.10500701.1

Klimenko, M. V., Klimenko, V. V., Bessarab, F. S., Sukhodolov, T. V., Vasilev, P. A., Karpov, I. V., et al. (2019). Identification of the Mechanisms Responsible for Anomalies in the Tropical Lower Thermosphere/ionosphere Caused by the January 2009 Sudden Stratospheric Warming. *J. Space Weather Space Clim.* 9, A39. doi:10.1051/swsc/2019037

Krall, J., Emmert, J. T., Sassi, F., McDonald, S. E., and Huba, J. D. (2016a). Day-to-day Variability in the Thermosphere and its Impact on Plasmasphere Refilling. *J. Geophys. Res. Space Phys.* 121, 6889–6900. doi:10.1002/2015JA022328

Krall, J., Glocer, A., Fok, M.-C., Nossal, S. M., and Huba, J. D. (2018). The Unknown Hydrogen Exosphere: Space Weather Implications. *Space Weather* 16, 205–215. doi:10.1002/2017SW001780

Krall, J., Huba, J. D., Denton, R. E., Crowley, G., and Wu, T.-W. (2014). The Effect of the Thermosphere on Quiet Time Plasmasphere Morphology. *J. Geophys. Res. Space Phys.* 119, 5032–5048. doi:10.1002/2014JA019850

Krall, J., Huba, J. D., Jordanova, V. K., Denton, R. E., Carranza, T., and Moldwin, M. B. (2016b). Measurement and Modeling of the Refilling Plasmasphere during 2001. *J. Geophys. Res. Space Phys.* 121, 2226–2248. doi:10.1002/2015JA022126

Krall, J., and Huba, J. D. (2019b). Simulation of Counterstreaming H+ Outflows during Plasmasphere Refilling. *Geophys. Res. Lett.* 46, 3052–3060. doi:10.1029/2019GL082130

Krall, J., and Huba, J. D. (2019a). The Effect of Oxygen on the Limiting H Flux in the Topside Ionosphere. *J. Geophys. Res. Space Phys.* 124, 4509–4517. doi:10.1029/2018JA026252

Kuwabara, M., Yoshioka, K., Murakami, G., Tsuchiya, F., Kimura, T., Yamazaki, A., et al. (2017). The Geocoronal Responses to the Geomagnetic Disturbances. *J. Geophys. Res. Space Phys.* 122, 1269–1276. doi:10.1002/2016JA023247

Lawrence, D. J., Thomsen, M. F., Borovsky, J. E., and McComas, D. J. (1999). Measurements of Early and Late Time Plasmasphere Refilling as Observed from Geosynchronous Orbit. *J. Geophys. Res. Space Phys.* 104, 14691–14704. doi:10.1029/1998JA900087

Lei, J., Thayer, J. P., Forbes, J. M., Sutton, E. K., Nerem, R. S., Temmer, M., et al. (2008). Global Thermospheric Density Variations Caused by High-Speed Solar Wind Streams during the Declining Phase of Solar Cycle 23. *J. Geophys. Res. Space Phys.* 113, 1–8. doi:10.1029/2008JA013433

Lühr, H., Liu, H., Park, J., and Müller, S. (2011). *New Aspects of the Coupling between Thermosphere and Ionosphere, with Special Regards to CHAMP Mission Results.* Dordrecht: Springer Netherlands, 303–316. doi:10.1007/978-94-007-0326-1_22

Makela, J. J., Baughman, M., Navarro, L. A., Harding, B. J., Englert, C. R., Harlander, J. M., et al. (2021). Validation of ICON-MIGHTI Thermospheric Wind Observations: 1. Nighttime Red-Line Ground-Based Fabry-Perot Interferometers. *J. Geophys. Res. Space Phys.* 126, e2020JA028726. doi:10.1029/2020JA028726

McCormack, J., Hoppel, K., Kuhl, D., de Wit, R., Stober, G., Espy, P., et al. (2017). Comparison of Mesospheric Winds from a High-Altitude Meteorological Analysis System and Meteor Radar Observations during the Boreal winters of 2009–2010 and 2012–2013. *J. Atmos. Solar-Terrestrial Phys.* 154, 132–166. doi:10.1016/j.jastp.2016.12.007

McDonald, S. E., Sassi, F., and Mannucci, A. J. (2015). Sami3/SD-WACCM-X Simulations of Ionospheric Variability during Northern winter 2009. *Space Weather* 13, 568–584. doi:10.1002/2015SW001223

McIlwain, C. E. (1961). Coordinates for Mapping the Distribution of Magnetically Trapped Particles. *J. Geophys. Res.* 66, 3681–3691. doi:10.1029/JZ066i011p03681

Millan, R., and Thorne, R. (2007). Review of Radiation belt Relativistic Electron Losses. *J. Atmos. Solar-Terrestrial Phys.* 69, 362–377. doi:10.1016/j.jastp.2006.06.019

Nossal, S. M., Mierkiewicz, E. J., and Roesler, F. L. (2012). Observed and Modeled Solar Cycle Variation in Geocoronal Hydrogen Using NRLMSISE-00 Thermosphere Conditions and the Bishop Analytic Exosphere Model. *J. Geophys. Res. Space Phys.* 117, 3311. doi:10.1029/2011JA017074

Oberheide, J., Pedatella, N. M., Gan, Q., Kumari, K., Burns, A. G., and Eastes, R. W. (2020). Thermospheric Composition O/N Response to an Altered Meridional Mean Circulation during Sudden Stratospheric Warmings Observed by GOLD. *Geophys. Res. Lett.* 47, e2019GL086313. doi:10.1029/2019GL086313

Ozhogin, P., Song, P., Tu, J., and Reinisch, B. W. (2014). Evaluating the Diffusive Equilibrium Models: Comparison with the IMAGE RPI Field-Aligned Electron Density Measurements. *J. Geophys. Res. Space Phys.* 119, 4400–4411. doi:10.1002/2014JA019982

Park, C. G. (1970). Whistler Observations of the Interchange of Ionization between the Ionosphere and the Protonosphere. *J. Geophys. Res.* 75, 4249–4260. doi:10.1029/JA075i022p04249

Picone, J. M., Emmert, J. T., and Lean, J. L. (2005). Thermospheric Densities Derived from Spacecraft Orbits: Accurate Processing of Two-Line Element Sets. *J. Geophys. Res. Space Phys.* 110, A03301. doi:10.1029/2004JA010585

Picone, J. M., Hedin, A. E., Drob, D. P., and Aikin, A. C. (2002). NRLMSISE-00 Empirical Model of the Atmosphere: Statistical Comparisons and Scientific Issues. *J. Geophys. Res. Space Phys.* 107, 1–16. doi:10.1029/2002JA009430

Pierrard, V., and Stegen, K. (2008). A Three-Dimensional Dynamic Kinetic Model of the Plasmasphere. *J. Geophys. Res. Space Phys.* 113, 1–15. doi:10.1029/2008JA013060

Qian, L., Burns, A. G., Solomon, S. S., Smith, A. K., McInerney, J. M., Hunt, L. A., et al. (2018). Temporal Variability of Atomic Hydrogen from the Mesopause to the Upper Thermosphere. *J. Geophys. Res. Space Phys.* 123, 1006–1017. doi:10.1002/2017JA024998

Qin, J., Waldrop, L., and Makela, J. J. (2017). Redistribution of H Atoms in the Upper Atmosphere during Geomagnetic Storms. *J. Geophys. Res. Space Phys.* 122, 10686–10693. doi:10.1002/2017JA024489

Richards, P. G., and Torr, D. G. (1985). Seasonal, Diurnal, and Solar Cyclical Variations of the Limiting H Flux in the Earth's Topside Ionosphere. *J. Geophys. Res. Space Phys.* 90, 5261–5268. doi:10.1029/JA090iA06p05261

Rishbeth, H. (1998). How the Thermospheric Circulation Affects the Ionospheric F2-Layer. *J. Atmos. Solar-Terrestrial Phys.* 60, 1385–1402. doi:10.1016/S1364-6826(98)00062-5

Roble, R. G., and Ridley, E. C. (1994). A Thermosphere-Ionosphere-Mesosphere-Electrodynamics General Circulation Model (TIME-GCM): Equinox Solar

Cycle Minimum Simulations (30–500 Km). *Geophys. Res. Lett.* 21, 417–420. doi:10.1029/93GL03391

Singh, N., and Horwitz, J. L. (1992). Plasmasphere Refilling: Recent Observations and Modeling. *J. Geophys. Res. Space Phys.* 97, 1049–1079. doi:10.1029/91JA02602

Stancil, P. C., Schultz, D. R., Kimura, M., Gu, J.-P., Hirsch, G., and Buenker, R. J. (1999). Charge Transfer in Collisions of O with H and H with O. *Astron. Astrophys. Suppl. Ser.* 140, 225–234. doi:10.1051/aas:1999419

Waldrop, L. S., Kudeki, E., González, S. A., Sulzer, M. P., Garcia, R., Butala, M., et al. (2006). Derivation of Neutral Oxygen Density under Charge Exchange in the Midlatitude Topside Ionosphere. *J. Geophys. Res. Space Phys.* 111, 1–14. doi:10.1029/2005JA011496

Wang, Y., Tu, J., and Song, P. (2015). A New Dynamic Fluid-Kinetic Model for Plasma Transport within the Plasmasphere. *J. Geophys. Res. Space Phys.* 120, 8486–8502. doi:10.1002/2015JA021345

Zawdie, K. A., Dhadly, M. S., McDonald, S. E., Sassi, F., Coker, C., and Drob, D. P. (2020). Day-to-day Variability of the Bottomside Ionosphere. *J. Atmos. Solar-Terrestrial Phys.* 205, 105299. doi:10.1016/j.jastp.2020.105299

Zoennchen, J. H., Nass, U., Fahr, H. J., and Goldstein, J. (2017). The Response of the H Geocorona between 3 and 8 to Geomagnetic Disturbances Studied Using TWINS Stereo Lyman-α Data. *Ann. Geophysicae* 35, 171–179. doi:10.5194/angeo-35-171-2017